Chapter 5

# Improving Contact Load-Bearing Resistance of Ultrafine-Grained Materials Through Multilayering and Grading

Dengke Yang, Jiangting Wang, Huimin Yang and Peter Hodgson

Additional information is available at the end of the chapter

http://dx.doi.org/10.5772/intechopen.72197

**Abstract**

Structural multilayering and grading has been designed to improve the contact load-bearing resistance of ultrafine-grained materials. The contact load-bearing response and surface damage resistance of multilayered hierarchical structured (MHSed) Ti were evaluated by experimental indentation on the overall loading response in conjunction with detailed computational simulations of local stresses and strain distribution. The combination of a hard outer layer, a gradual transition layer and a compliant core results in reduced indentation depth, but a deeper and more diffuse sub-surface plastic deformation zone, compared to the monolithic nanostructured Ti. The macroscopic indentation resistance of MHSed Ti is controlled by the underlying micromechanics of the multilayered hierarchical structure. The finite element analysis (FEA) revealed the multilayered hierarchical structure offers the effective macroscopic mechanical contact loading resistance, where the indenter increasingly "senses" the more compliant core to bear the deformation as the load increases. The structural multilayering modifies the stress and strain redistribution and effectively reduces the maximum stress concentration within the material. The structural grading provide a transitional junction for stress and plastic deformation redistribution and achieve more gradual stress distributions between component layers which mitigates the interface failure, increases the interfacial toughness, thus providing strong resistance to loading damage.

**Keywords:** ultrafine-grained materials, multilayered hierarchical structure, multilayering, grading, contact load-bearing resistance, finite element modeling

## 1. Introduction

Materials with high contact damage resistance are extensively required in aerospace and aircraft, vehicle industry, microelectro-mechanical systems and devices, cutting tools and bulletproof vests [1, 2]. An approach for improved resistance to surface contact damage is to design surface gradations in composition, microstructure and elastic and/or plastic properties [2–4]. Such design provide effective means to enhance materials contact damage resistance through redistribution of thermal and/or mechanical stresses, elimination of interface-induced stress concentrations and reduction in the local crack driving force [5–8]. Nature is a master in the design of sophisticated hierarchical structured materials which provide excellent damage resistance [9]. A typical example is the material structural design principle found in a fish armor [10]. In response to predatory threats, fish are protected by armor scales consisting of four distinct reinforcing layers of organic/inorganic nanocomposites with hardness and modulus decreasing gradually from the outer to the inner layers. The juxtaposition of multiple reinforcing composite layers and the gradations, both in microstructure and mechanical properties within and between material layers, provides a more compliant protective mechanism than the monolithic counterpart [10].

Inspired from the material structural design principle discovered in natural/biological systems, materials scientists have generated enormous interest in replicating natural/biological structures with excellent damage resistance than their conventional counterparts. Over the past 2 decades, significant progress has been made in synthesis and fabrication of materials with graded properties over multiple length scales. Elastically graded materials (EGMs), where the materials have gradient in elastic modulus as a function of depth beneath the surface, were synthesized by controlled infiltration of aluminosilicate or oxynitride glass into polycrystalline ceramic matrix, which offered superior resistance to contact damage than either constituent ceramic matrix or glass [11–13]. Plastically graded materials (PGMs) were produced by increasing or decreasing the grain size within the nanocrystalline or microcrystalline range to create a linear gradation of yield strength as a function of depth below the material surface according to classical Hall–Petch effect [3]. The benefit of the gradient effect on the stress–strain and deformation response under normal indentation have been demonstrated by analytical [14], computational [15–17] and experimental studies [18, 19].

In our recent work [20], we extended the EGM/PGM concept to design a multilayered hierarchical structure (MHS) on Ti. By the application of Surface Mechanical Attrition Treatment (SMAT) [21] to cryorolled Ti, a three-layered structure formed consisting of an outer amorphous/nanocrystallite (A/NC) layer, an inner nanograined (NG) layer and ultrafine-grained (UFG) core [20]. Nanoindentation through the cross-section of the multilayered hierarchical structured (MHSed) Ti revealed a gradual decrease in hardness and modulus within and between each successive structural layer [20]. These properties correlate with the microstructure characteristics and the design principle found in natural systems, such as fish armor [10]. The work hardening of the MHSed Ti was improved largely by such structural design [20]. Moreover, the gradations in structure and properties, pore and crack-free nature and the inherently damage tolerant top A/NC layer of MHSed Ti are expected to benefit the contact deformation and damage resistance of MHSed Ti.

Studies of the effects of microstructural, compositional, and property gradients on the overall elastic–plastic response under contact loading are an area of great interest, and much progress has been achieved in the fundamental understanding of graded surface damage resistance [2]. However, systematic investigations of the multilayered hierarchical structure on indentation response, contact damage resistance and contact surface failure of graded ultrafine-grained (UFG) metal, in particular with regards to the structural multilayering and grading, have not been investigated by multiscale experimental and computational approaches and the mechanism of the contact load-bearing response in these situations is also largely unknown.

In this Chapter, we focus on the contact load-bearing response and surface damage resistance of MHSed Ti relative to monolithic nanostructured Ti. Through experimental investigations and computational simulations of local stress and strain distributions, the mechanism of the contact load-bearing response of MHSed Ti is explored. These results provide clear evidence of improved contact load-bearing capacities through structural multilayering and grading. Such information is of practical value for the design of UFG materials with excellent contact load-bearing capacities for engineering applications.

## 2. Experimental procedures

The MHSed Ti was produced by the following experimental procedures. A commercial Ti plate (Grade 2) with 36 mm in thickness was cryogenically rolled to 5 mm with per reduction of ~2 mm. The detailed microstructure characterizations of the cryorolled Ti have been given elsewhere [22]. The cryorolled workpiece then was cut parallel to the rolling direction (RD) to a rectangular bar with dimensions of $5 \times 5 \times 90$ mm$^3$. Subsequently, one lateral surface of the rectangular bar was subjected to SMAT. The SMAT process was performed in a low vacuum condition using hardened stainless steel balls (8 mm in diameter) at a vibration frequency of 50 Hz for 60 min. The detailed MHS process can be found in [20]. The production of monolithic NG Ti has been given in [22].

**Figure 1a** shows a schematic illustration of the nanoindentation and contact load-bearing testing. Nanoindentation experiments were carried out at ambient temperature using an UMIS indentation system with a Berkovich diamond tip at a strain rate of $5 \times 10^{-2}$ s$^{-1}$ and a maximum load of 20 mN. Before testing, the cross-sectional surface was polished to 0.5 μm diamond suspension finish. The values of the nanoindentation hardness and modulus quoted here were the average of 10 measurements on the cross-sectional surface. Before Vickers microhardness and load-bearing testing, artifacts on the surface caused by MHS process were carefully removed by polishing to 0.5 μm diamond suspension finish (removal thickness < 2 μm). Vickers microhardness testing was conducted using a microhardness tester (FM 700) under a load of 0.5, 1, 3, 5, 10 N on the MHSed surface at more than 10 points and the average values were reported here. Load-bearing testing was conducted with a spherical tungsten carbide (WC) indenter with diameter of 1.5 mm in ambient conditions. The WC indenter had an elastic modulus of 640 GPa and a Poisson's ratio of 0.26. The indenter came into contact with the specimen surface and was loaded to a maximum load of 1000 N at a loading rate of 1000 N/s.

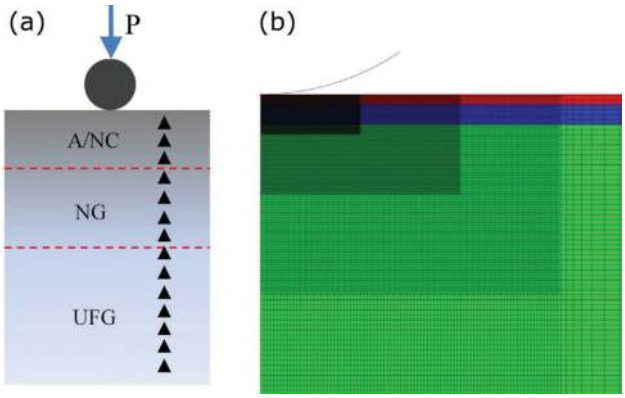


**Figure 1.** (a) Schematic illustration of the surface load-bearing and cross-sectional nanoindentation testing. The black ball represents the load-bearing testing indenter and the black triangle represents the indent of nanoindentation testing. (b) Finite element mesh of the ball indentation model.

Microstructural and damage observations were conducted using a field-emission gun scanning electron microscope (SEM) Zeiss Supra 55VP operated at 10 kV and a transmission electron microscope (TEM) Jeol JEM 2100 operated at 200 kV.

A two-dimensional axisymmetric model was developed to simulate the ball indentation using Abaqus v6.10. The specimens were modeled as isotropic, elastic–perfectly plastic following the large-deformation theory. The finite element mesh contained 42,163 four-node bilinear axisymmetric quadrilateral elements (CAX4R), with a refined mesh in the indentation region (**Figure 1b**). Mesh convergence was verified by comparing load–depth curves and stress contours using models with element number ranging from 11,183 to 42,163. A user subroutine UMAT was developed to take into account the gradation of material properties, in which the discrete and gradient model parameters were assigned to elements based on their distance from the surface (see later for further details). The ball indenter was modeled as a rigid body, and the contact between the indenter and specimen was assumed frictionless. A maximum load of 1000 N was applied to indent the samples at a loading rate of 1000 N/s. The finite element analysis (FEA) of the microindentation adopted a similar methodology to the axisymmetric nanoindentation simulations. The Vickers indenter was modeled to be a conical rigid indenter with an apex angle of 70.3° and tip radius of 3.4 μm, which approximates a Vickers indenter tip.

## 3. Results

### 3.1. Microstructure

A SEM cross-sectional view of the MHSed Ti surface shows three-layered structure without sharp interfaces between the successive layers (**Figure 2a**). TEM analysis revealed that the ~30 μm thick top layer was composed of a bright phase matrix and a discrete darker nanostructure (**Figure 2b**).

The upper right inset taken from the bright matrix region exhibited a broad diffuse halo in a selected-area diffraction pattern (SAD), which is typical of a fully amorphous phase. The SAD pattern in the lower left inset taken from the interface between the bright and dark phases clearly demonstrates the presence of a nanocrystalline phase together with the amorphous phase. The NG layer (~60 μm thick), situated beneath the A/NC layer, consisted of nanograins (**Figure 2c**). The corresponding SAD pattern shows a ring pattern, demonstrating the nanostructure has random crystallographic orientations. The size of the nanograins was in the range from 5 to 80 nm with an average size of ~40 nm (**Figure 2e**). The UFG core is composed of ultrafine equiaxed grains with a grain size distribution of 50–250 nm (**Figure 2d** and **f**).

### 3.2. Mechanical gradations

Nanoindentation was used to measure the elastic and plastic mechanical properties spatially through the cross-section of the MHSed Ti. The elastic mismatch and delamination, commonly existed in other multilayered systems produced by deposition or coating, are two critical factors controlling crack confinement [23]. In contrast, due to the gradients in both the strain and strain rate induced by the cryorolling and SMAT process from the top surface to the inner core, the reported MHSed Ti is free from elastic mismatch and delamination between layers.

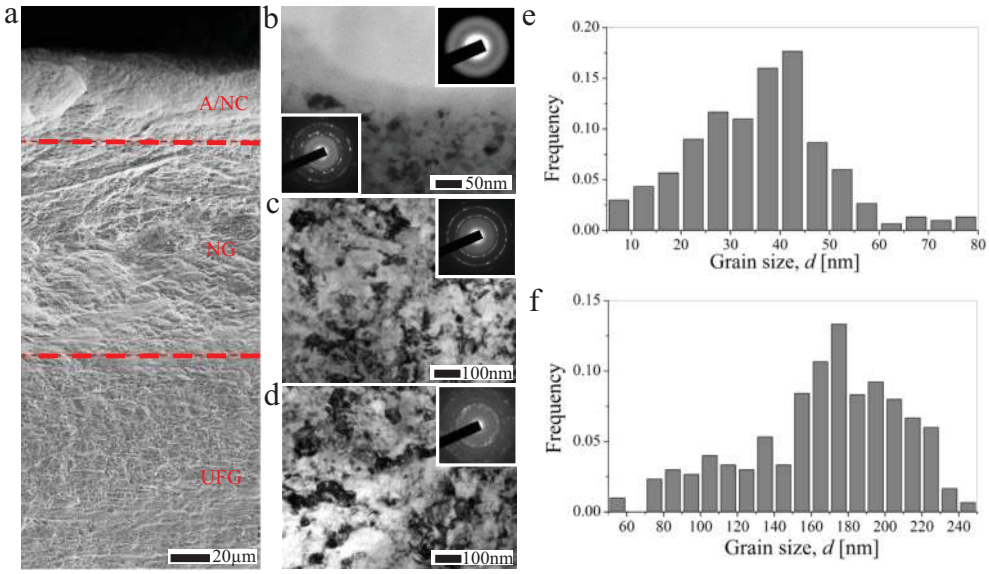


**Figure 2.** Microstructural characteristic of the MHSed Ti: (a) SEM cross-sectional image. (b) TEM bright-field (BF) image of the microstructure situated 20 μm below the top surface. The upper right and lower left insets are the selected-area diffraction (SAD) patterns of the bright region the dark region, respectively; (c) TEM BF image of the microstructure located 60 μm below the top surface. The inset shows the corresponding SAD pattern; (d) TEM BF image of the innermost core. The inset shows the corresponding SAD pattern; (e and f) histogram of the grain size distribution in the NG layer (e) and UFG core (f). The grain size $D$ was defined by $D = \sqrt{d_T \times d_L}$, $d_T$ is the transverse length of the grain and $d_L$ is the longitudinal length. 300 grains were statistical measured from several TEM dark-field (DF) images.

Moreover the MHSed Ti possesses mechanical gradations within and between each successive layer. The Oliver–Pharr [24] indentation hardness $H_{O-P}$ (ranging from ~5.3 to ~3.2 GPa) and modulus $E_{O-P}$ (ranging from ~137 to ~113 GPa) gradually decreased with the distance from the top surface to the core (**Figure 3a** and **b**). The highest average indentation hardness (~5.2 GPa) of the top A/NC layer is consistent with its microstructure which is composed of amorphous and nanocrystalline phases. The NG layer has nanograins compared with the A/NC layer, but reduced grain size relative to the UFG core, consistent with the mechanical trend observed in **Figure 3a** and **b**. The UFG core, consists of ultrafine equiaxed grains with average grain size of ~180 nm, thus has the lowest average indentation hardness (~3.2 GPa). **Figure 3c** shows the SEM image of the residual indents after indentation unloading. The absence of radial or circumferential cracks confirms the plastic nature of the material layers. The mechanical gradations were calculated as the slope of datasets presented in **Figure 3a**. With the distance from the outer surface to inner core, approximately negative linear gradations in both $E_{O-P}$ and $H_{O-P}$ were obtained within the top A/NC and the NG layers beneath. The UFG core, however, show no detectable gradation. **Table 1** summarizes the gradations of $E_{O-P}$ and $H_{O-P}$ in each layer.

### 3.3. Contact load-bearing response

The experimental contact load-bearing response of the MHSed Ti and the monolithic NG Ti is shown in **Figure 4**. For the same contact load (1000 N), a relatively small contact impression

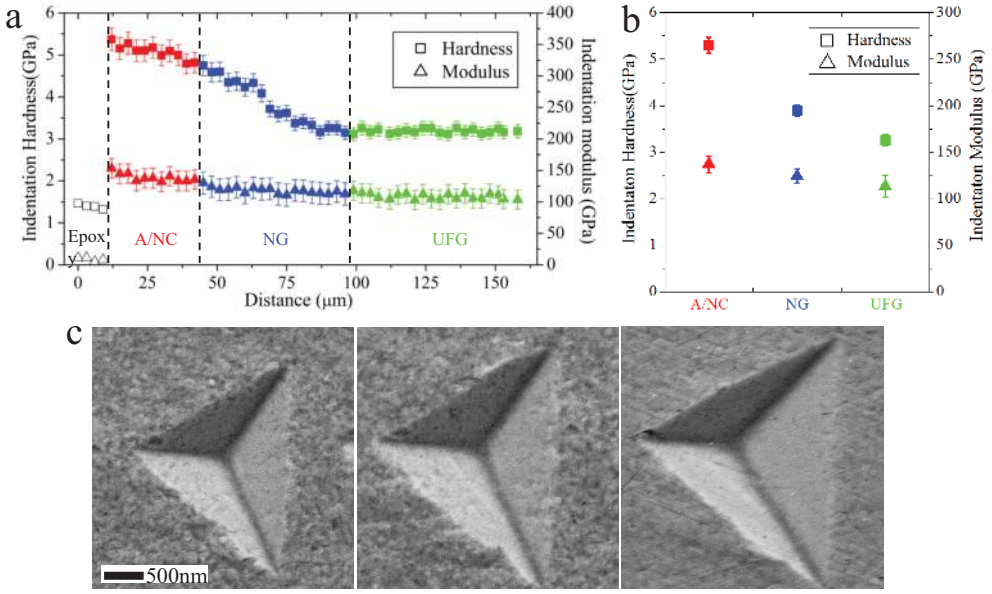


**Figure 3.** Mechanical gradations of the MHSed Ti. (a) Hardness and modulus through the cross-section of MHSed Ti using a 20 mN maximum load; (b) average indentation hardness and modulus for each of the layers; and (c) SEM images of the residual indents on the cross-section of each layer. From left to right: A/NC, NG, and UFG.

| Components (layer) | Gradation $E_{O-P}$ (GPaμm$^{-1}$) | Gradation $H_{O-P}$ (GPaμm$^{-1}$) |
|---|---|---|
| A/NC | −0.57 | −0.013 |
| NG | −0.25 | −0.014 |
| UFG | 0 | 0 |

**Table 1.** Mechanical gradations in each component layer.

for the MHSed Ti is expected due to the high hardness and strength of the top A/NC layer. The residual impression radius for the MHSed Ti and the monolithic NG were measured to be 424 and 488 μm (**Figure 4a** and **b**), respectively. A complete suppression of cracks in the MHSed material was clearly substantiated by SEM observations (**Figure 4c**). In contrast, cracks (marked by white arrows) appeared to initiate at the contact edge of the indentation and propagate through the region in the monolithic NG Ti, most likely due to local stress concentrations (**Figure 4d**).

Most of the plastic deformations of the tested materials occur within a semi-circular area as revealed by optical microscopy observation on the cross sections (**Figure 4e–h**). The semi-circle represents an elastic–plastic deformation border and the semi-circular area can be considered as the plastic strain zone. The overall through-thickness impact impression of the MHSed Ti is comparatively much lower (**Figure 4c**) than the monolithic NG Ti (**Figure 4d**), however, the MHSed Ti yields a significant compliance and the elastic–plastic deformation border occurs at a greater depth compared with the monolithic NG material (**Figure 4e** and **f**). The radius of the plastic strain zone for the MHSed Ti and monolithic NG Ti was established to be ~530 μm and ~460 μm, respectively. High magnification observations on the elastic–plastic strain boundary revealed that the MHSed Ti achieves more gradual strain redistribution than the monolithic NG Ti in which intense shear localization were found (**Figure 4g** and **h**). The smooth transitional region for elastic–plastic deformation in the MHSed materials is the direct result of the multilayered structure accommodating the imposed load. These results suggest that the multilayered structure and the associated mechanical gradations in the material offer an advantageous mechanism for contact damage resistance.

### 3.4. Computational simulations

To better understand how the structural multilayering and grading influences the contact load-bearing behavior of the MHSed materials, an elastic–perfectly plastic finite element analysis (FEA) computational model was developed. Here the three-dimensional indenter geometry represented as two dimensional, axisymmetric and rigid has been simulated to fit the experimental nanoindentation loading-depth data for each layer. The extensive study showed that incorporating the post yield strain hardening (linear isotropic, linear kinematic and Ramberg–Osgood isotropic hardening) into the models had a minimal effect on improving the prediction of the simulated data and the estimated yield strength [10]. Consequently, we assume zero hardening for plastic behavior and that the material deformation is elastic–perfectly plastic. This is a simple and effective approach to describe the mechanical behavior of the material.

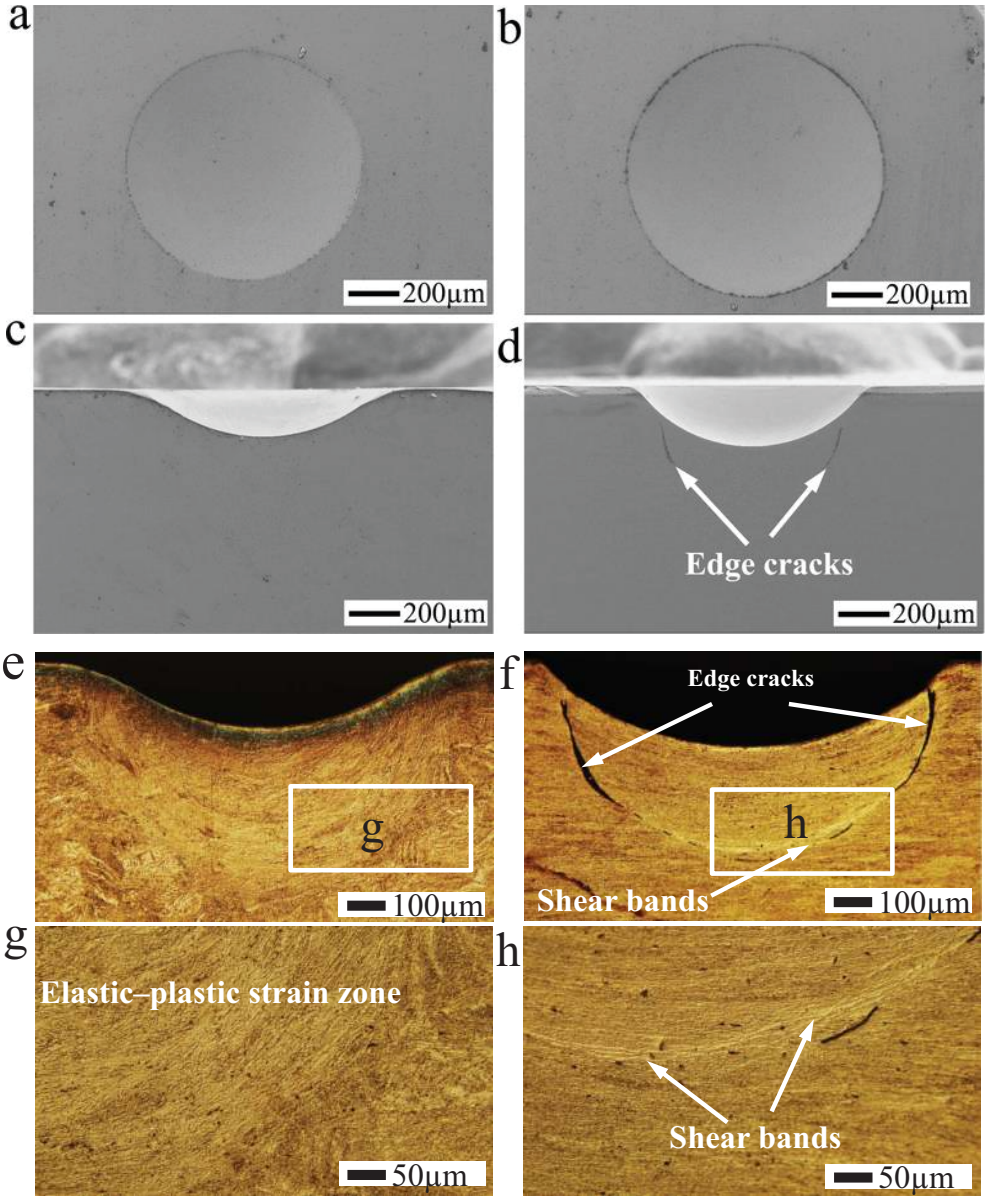


**Figure 4.** SEM and OM images of indentation testing results of the MHSed Ti and monolithic NG Ti. (a and b) Top surface SEM views of the MHSed Ti and monolithic NG Ti, respectively. (c and d) Cross-sectional view of the MHSed Ti and monolithic NG Ti, respectively. (e and f) OM cross-sectional views of the plastic deformed area in the MHSed Ti and monolithic NG Ti, respectively. (g and h) HR OM images of the boundary of elastic–plastic strain zone for the MHSed Ti and monolithic NG Ti, respectively.

In these simulations, the FEA-predicted unloading slope was selected to match the experimentally calculated average $E_{O-P}$ for each layer (**Figure 3b**). Various material yield strengths ($\sigma_Y$) were chosen to determine the optimal value at which the FEA-predicted load and unload–depth curve best fits the experimental load and unload–depth curve. The averaged experimental load–depth curves (solid line in **Figure 5**) were selected from the experimental nanoindentation load–depth curve dataset, whose unloading slope represents the average indentation modulus for each layer presented in **Figure 3b**. In the initial simulations, the yield strength of each layer was based on results from our earlier work using micro-compression testing [20]. Using such yield strength, the simulated load–depth curve (dash line in **Figure 5**) was obtained and compared to the averaged experimental curve. By adjusting the yield strength value and iteratively repeating the simulations until the simulated and experimental curves correlated (**Figure 5**), the yield strength for each layer was determined. **Figure 5** shows the FEA simulations best fit the averaged experimental load–depth curve for each component layer. All the component layers exhibit mechanical hysteresis and energy dissipation (calculated as the area of the average experimental load–depth curves), which increased with the distance from the outer layer. The good agreement between the experimental data and the computational simulations gives the material yield strength $\sigma_Y$ values of 1.76, 1.38 and 1.15 GPa for the A/NC layer, the NG layer and the UFG core, respectively.

In our FEA simulations, the effects of the structural multilayering and grading on the large-length-scale mechanical indentation of the MHSed Ti were explored by constructing two axisymmetric two-dimensional FEA models. The first "discrete" model consisted of a MHS of three

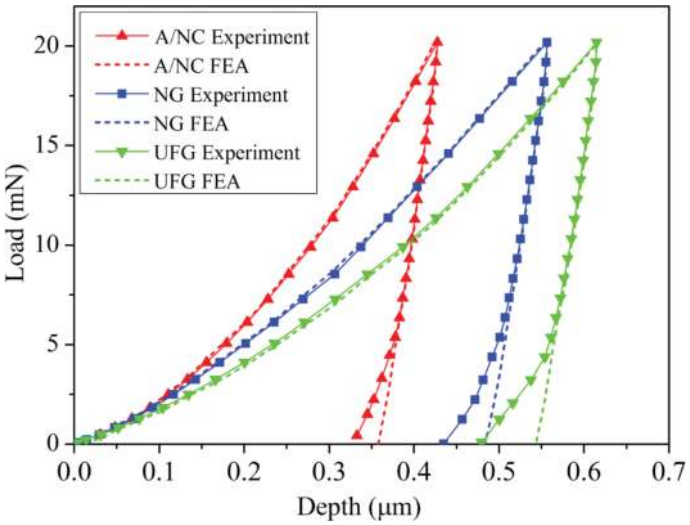


**Figure 5.** Experimental and FEA simulated average nanoindentation load–depth curves for the A/NC, NG layers and the UFG core.

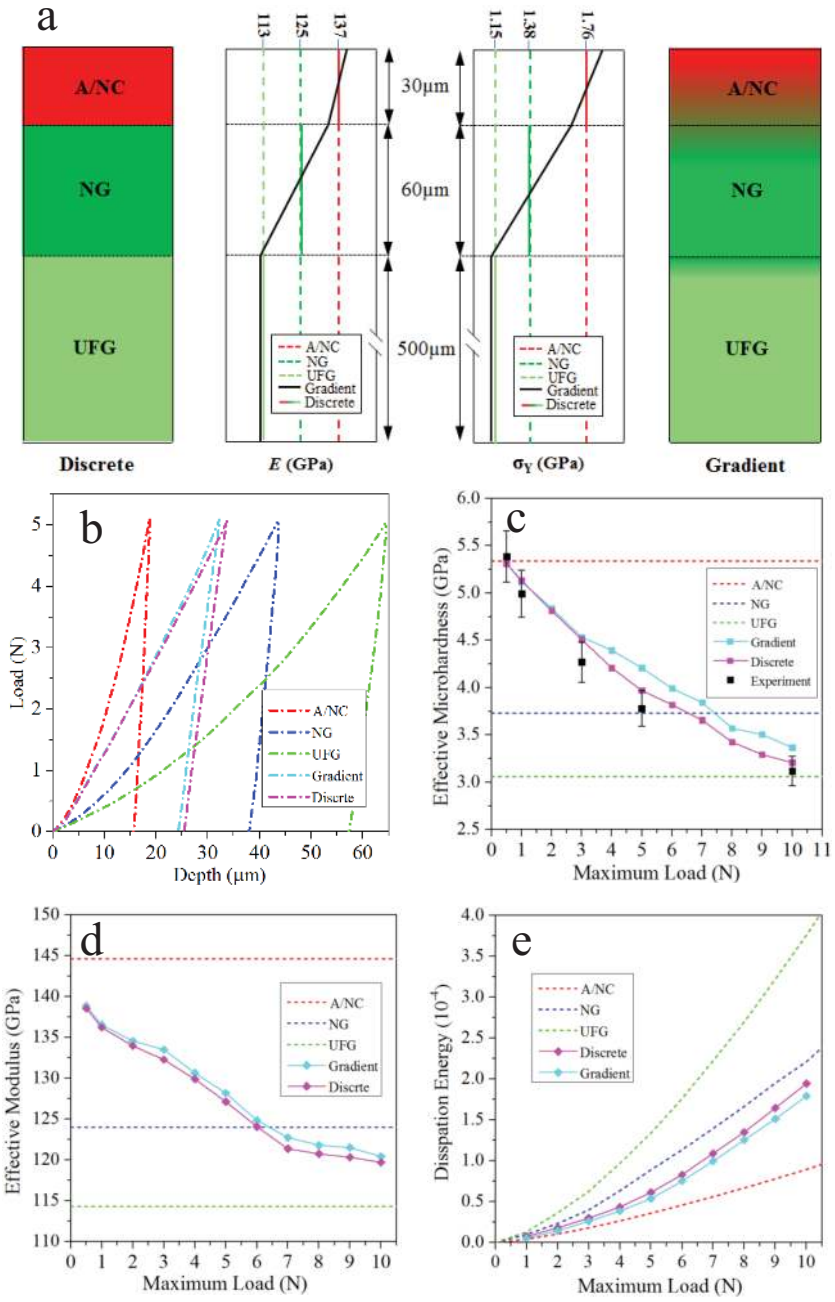


**Figure 6.** (a) FEA simulated models of discrete (left) and gradient (right) multilayered structure, the corresponding elastic modulus and yield strength distributions are presented in the center. (b) FEA simulated microindentation load–depth curves for different component layer and two models (discrete and gradient), (c) simulated effective microhardness and experimentally measured values, (d) simulated effective indentation modulus, and (e) simulated effective energy dissipation.

http://dx.doi.org/10.5772/intechopen.72197

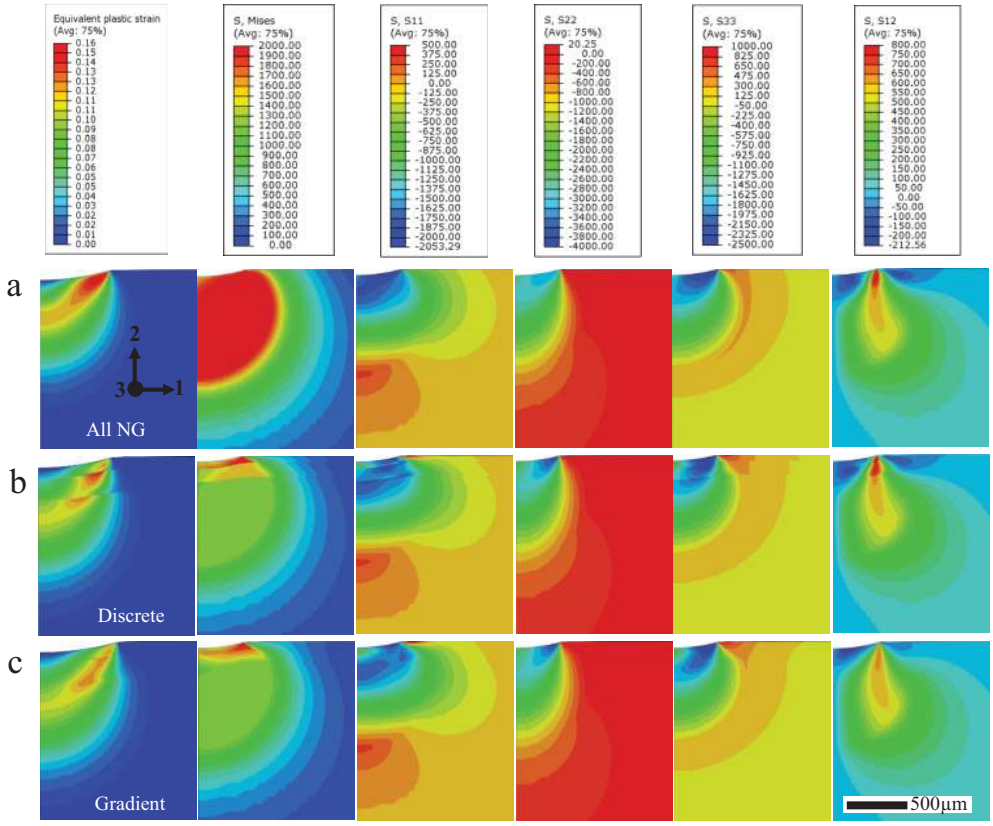


**Figure 7.** The simulated strain and stress contours for 1000 N maximum load indentation. (a) Monolithic NG, (b) discrete model, and (c) gradient model. $S_{ii}$ ($i$ = 1–3) represents the normal stress along $i$ axis, and $S_{12}$ is the shear stress that is in the plane perpendicular to the 1 axis and acts along the 2 axis.

layers with thicknesses matching their experimentally measured values (**Figure 6a**, left). In the discrete model, each layer was assumed to possess isotropic, elastic–perfectly plastic constitutive behavior with $E$ and $\sigma_Y$ taken as those calculated from FEA simulations of the averaged loading-depth data in **Figure 5**. The second "gradient" model is also composed of the three component layers with thickness corresponding to their experimental values and assumed isotropic elastic–perfectly plastic material property, but incorporates linear gradations (**Table 1**) in $E$ (scaled by the measured $E_{O–P}$ gradation) and $\sigma_Y$ (scaled by the measured $H_{O–P}$ gradation) within the material layers (**Figure 6a**, right). **Figure 6b** shows the FEA simulation results of these two models compared with three simulations of the single homogeneous component layer of the A/NC, NG layers and the UFG core. The predications of these two multilayered models show similar load–depth behavior and both fell in between the simulation of the A/NC and the NG layers.

Based on the FEA simulations, the mechanical behavior of the MHS material was explored by deducing each load–depth performance to an effective O–P modulus, effective microhardness and energy dissipation. The effective modulus and hardness predicted for the two models

(discrete and gradient systems) showed a loading-dependency, which is not the case for the single homogeneous systems (**Figure 6c** and **d**). The effective modulus and hardness for discrete and gradient systems decreased nonlinearly between that of the A/NC layer at small loads and the values corresponding to UFG core at maximum load of 10 N. Good agreement in the magnitude and the load dependency was achieved between the effective hardness and the experimentally measured microhardness (**Figure 6d**). The effective energy dissipation of these two models was found to increase with increasing load and all fell in between the A/NC layer and the UFG core (**Figure 6e**).

### 3.5. Strain and stress simulation

The contact load-bearing behavior of the MHSed Ti was further assessed using FEA to simulate the stress and strain distributions within the materials. **Figure 7** shows the stresses and corresponding equivalent plastic strain contours after unloading (maximum load of 1000 N) for the simulated multilayered systems (discrete and gradient) as compared with that of the monolithic NG material. As presented by the color contours, both the stresses and the equivalent strains exhibit graded distributions within the gradient model, as opposed to the abrupt changes observed in the discrete model. The maximum magnitude of equivalent plastic strain in the monolithic NG material (0.17) is greater than those in both the discrete and gradient multilayers (0.14 and 0.13, respectively). However, the multilayered models (discrete and gradient) achieve deeper and a broader plastic deformation field than that of the monolithic NG material. These simulations further suggest that the structural multilayering and grading modified the stress and strain distribution and reduce the overall plastic strain level throughout the material under indentation conditions.

## 4. Discussion

### 4.1. Structural multilayering

The present experimental studies show the plastic deformed area for the MHSed material was markedly greater than that for monolithic NG (**Figure 4**) and this is consistent with the results obtained from FEA microindentation simulations, where the indenter increasingly induces the more compliant UFG core as the load increases (**Figure 6c** and **d**). Further FEA simulations showed that the degree of energy dissipation (occurring by the inelastic deformation) of multilayered cases (discrete and gradient) increased with increasing load (**Figure 6e**). These results indicate that the macroscopic indentation behavior was directly governed by the underlying micromechanics of the multilayered structure. The load–depth FEA simulations (**Figure 6**) revealed that there was negligible difference in the load–depth response for the discrete and gradient models, suggesting that it is the overall structural multilayering that provides the effective macroscopic mechanical loading resistance rather than the grading.

Recent experimental nanoindentation studies, supported by cross-sectional electron microscopy observations, revealed that the multilayered structures provide a higher resistance to deformation than monolithic counterparts [25–27]. FEA simulations indicated that the structural layering

http://dx.doi.org/10.5772/intechopen.72197

modified the stress distribution and reduced the overall strain values, suppressing crack formation [28]. In our present study, the multilayered models (discrete and gradient) showed a considerable redistribution of the overall equivalent plastic strain field and a significant reduction in the maximum strain levels (**Figure 7**). The plastic equivalent strain contours revealed an increased depth and strain area of plastic deformation for the multilayered systems compared with the monolithic NG material. This is a direct result of transferring the plastic strain to the underlying UFG core with a lower $\sigma_Y$ than the NG layer, thereby diffusing the total plastic deformation energy. The FEA results coincide with the experimental results presented in **Figure 4** where the MHSed Ti diffuses plastic deformation over a greater region relative to the monolithic NG Ti.

### 4.2. Mechanical grading

The discrete and gradient models were shown to achieve similar macroscopic effective indentation modulus and microhardness (**Figure 6**). However, FEA simulations revealed differences in the stress and plastic equivalent strain distributions between gradient and discrete models after unloading (**Figure 7**). The magnitude of the equivalent plastic deformation in the top A/NC and NG layers in the gradient system is lower than that experienced in the discrete system. Further, the magnitude and area of plastic deformation in the UFG core are greater in the gradient system compared with the discrete system. This result reveals that the reduction in the stresses and plastic deformation in the top layers is a direct consequence of the increased deformation and energy dissipation accommodated by the softer inner UFG core. Moreover, the mechanical gradations in the successive layers and junctions are observed to give rise to more gradual stress redistribution between component layers, as opposed to the abrupt stress changes observed in the discrete model (**Figure 8**). Such graded stress distribution is believed to lessen the interface failure and increase the interfacial toughness, thus providing strong resistance to loading-damage [10, 29].

The different transition patterns between elastic and plastic deformation shown in **Figure 6** are consistent with the FEA simulation results. The smooth transitional region in the MHSed Ti is attributed to its graded stress distribution achieved by microstructural grading. The absence of any interfacial failure, such as delamination or fracture, observed between the layers in the

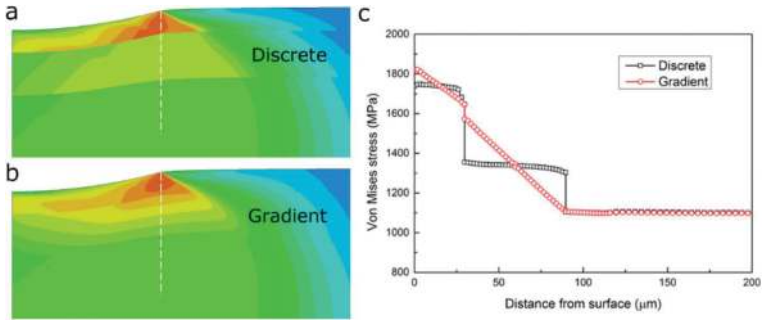


**Figure 8.** Distribution of Von Mises stress under the indentation regions in (a) discrete and (b) gradient models, while (c) shows the Von Mises stresses across the interfaces along the white dotted lines.

MHSed Ti under indentation further confirms that mechanical gradations provide resistance to interfacial failures. The smaller magnitude of the stresses and plastic deformation within the "stiffer" top layers and the greater plastic deformation in "softer" inner UFG core for the gradient system diffuse the total plastic deformation energy and offer a suppression to strain localization which occurred in the monolithic NG Ti (**Figure 4h**).

### 4.3. Cracks and stress concentrations

Identifying the linkage between stress and strain concentration and the initiation of cracks experimentally observed is one of the most important issues in FEA analysis. There are three types of cracks in hard materials under indentation conditions: edge, radial and lateral shear cracks (also known as delamination) [26, 28]. Edge cracks begin at the contact edge of the indentation and extend into the material, and are associated with the local tensile and shear stresses [28]. Lateral shear cracks are the result of shear strain localization arising from the high shear stress during indentation testing [30]. Radial cracks generally initiate directly under the indentation and propagates in a direction parallel to the indentation at excessive radial stresses [28]. The cracks observed in the present study (**Figure 4d** and **f**) agree well with the stress concentrations predicted by FEA simulations (**Figure 7**). The location of the edge cracks observed experimentally in monolithic NG Ti are consistent with the tensile stress (S11) and shear stress (S12) locations where the maximum tensile stress and shear stress appear immediately below the indenter (**Figure 7**). However, within the MHSed Ti, the stress (S11 and S12) variation is more gradual, with the shear stress reduced by 38% (0.21–0.13 GPa) at the maximum stress location. Such stress distribution and stress magnitude reduction explains the experimental observation that edge cracks were absent from the MHSed Ti but clearly occurred in monolithic NG Ti. The shear stresses in monolithic NG Ti are distributed over the plastic deformation region and coincide with the sites where shear bands were experimentally observed. With regards to the MHSed Ti, the multilayering and grading reduce the magnitude of maximum shear stress (**Figure 7**), therefore, the shear localized deformation was absent in the MHSed Ti (**Figure 4g**). These analyses reveal that multilayering and grading can significantly modify the stress field and effectively reduced the maximum stress concentration within the materials, thereby reduce the probability of cracks and shear localization which was commonly experienced in monolithic materials under indentation condition.

### 4.4. Other aspects contribute to the contact load-bearing

Our previous study [31] using micropillar compression testing has shown the deformation-induced precipitation of nanocrystals in the outer A/NC layer. The interaction of microcracks and shear bands with these nanocrystals allowed high ductility in this layer. This plasticity was evident in the present study by the indentation-induced deformation in the A/NC layer (**Figure 4a** and **e**). Previous studies demonstrated that the inelastic deformation occurring in the graded ceramics can contribute toward the cone-crack suppression [11, 12]. The susceptibleness of the A/NC layer to deform plastically reduces the propensity for cracking under indentation condition.

Residual stress may also be contributing to crack suppression in the deformed MHSed Ti structure. Residual surface compressive stress can be induced by various techniques to improve the contact damage resistance and strength of many brittle materials [32]. Further, multilayering and mechanical grading of a surface is known produce complex residual stresses [33, 34]. The residual stress–depth profile analysis [20] revealed that the MHSed Ti has residual compressive stresses through the layers and a tensile stress at the NG layer/UFG core interface. The residual compressive stress in A/NC and NG layers act to arrest crack development and increase damage resistance, however the residual tensile stress at NG/UFG junction theoretically increases the propensity for crack initiation under contact loading. Given the absence of cracking at the NG/UFG interface, it appears the reduction of maximum stress and the attendant of redistribution of the stresses arising from multilayering and mechanical grading more than compensate for the residual tensile stress.

## 5. Summary and conclusions

In summary, we report on both the contact load-bearing response and underlying deformation mechanism for MHSed Ti using indentation testing in combination with detailed computational simulations of local stresses and plastic deformation strain distributions. The results provide evidence for enhanced contact load-bearing resistance and energy dissipation by introducing multilayers and mechanical gradations into the surface region of the UFG material. This material design strategy is expected to applicable to a broad class of metallic materials. The following conclusions can be drawn from this study:

(1) The MHSed Ti exhibited enhanced resistance to contact loading damage compared to the monolithic NG Ti. The multilayering and grading of UFG materials suppressed the formation of cracks and increased the loading damage resistance.

(2) The macroscopic indentation resistance of the MHSed Ti arises from the underlying micromechanics of the multilayered structure. The overall multilayered structure offers the effective macroscopic mechanical loading resistance, where the loading increasingly induces the more compliant structure to bear the deformation as the load increases.

(3) The mechanical gradation provides a transitional junction for stress redistribution and achieves a more gradual stress distribution between component layers. Such a graded stress distribution mitigates the interface failure and increases the interfacial toughness, thus providing strong resistance to loading damage.

(4) The microstructural multilayering and grading of UFG metal can significantly modify the stress field and effectively reduce the maximum stress concentration within the material, thereby reduce the probability of cracks and shear localization which are commonly experienced in monolithic materials under indentation conditions.

## Author details

Dengke Yang[1,2]*, Jiangting Wang[2], Huimin Yang[3] and Peter Hodgson[2]

*Address all correspondence to: dkyang@issp.ac.cn

1 School of Materials Science and Engineering, Anhui University of Technology, Anhui, China

2 Institute for Frontier Materials, Deakin University, Victoria, Australia

3 China National Bamboo Research Center, Zhejiang, China

## References

[1] Miyamoto Y, Kaysser WA, Rabin BH, Kawasaki A, Ford RG, editors. Functionally Graded Materials: Design, Processing and Applications. 1st ed. Boston: Springer US; 1999. 330 p. DOI: 10.1007/978-1-4615-5301-4

[2] Suresh S. Graded materials for resistance to contact deformation and damage. Science. 2001;**292**(5526):2447-2451. DOI: 10.1126/science.1059716

[3] Prasada A, Dao M, Suresh S. Steady-state frictional sliding contact on surfaces of plastically graded materials. Acta Materialia. 2009;**57**(2):511-524. DOI: 10.1016/j.actamat.2008.09.036

[4] Kieback B, Neubrand A, Riedel H. Processing techniques for functionally graded materials. Materials Science and Engineering: A. 2003;**362**(1-2):81-106. DOI: 10.1016/S0921-5093(03)00578-1

[5] Kesler O, Matejicek J, Sampath S, Suresh S, Gnaeupel-Herold T, Brand PC, Praskc HJ. Measurement of residual stress in plasma-sprayed metallic, ceramic and composite coatings. Materials Science and Engineering: A. 1998;**257**(2):215-224. DOI: 10.1016/S0921-5093(98)00860-0

[6] Giannakopoulos A, Suresh S. Indentation of solids with gradients in elastic properties: Part I. Point force. International Journal of Solids and Structures. 1997;**34**(19):2357-2392. DOI: 10.1016/S0020-7683(96)00171-0

[7] Suresh S, Giannakopoulos A, Olsson M. Elastoplastic analysis of thermal cycling: Layered materials with sharp interfaces. Journal of the Mechanics and Physics of Solids. 1994;**42**(6):979-1018. DOI: 10.1016/0022-5096(94)90081-7

[8] Chen AY, Li YK, Zhang JB, Pan D, Lu J. The influence of interface structure on nanocrystalline deformation of a layered and nanostructured steel. Materials & Design. 2013;**47**:316-322. DOI: 10.1016/j.matdes.2012.11.050

[9] Munch E, Launey ME, Alsem DH, Saiz E, Tomsia AP, Ritchie RO. Tough, bio-inspired hybrid materials. Science. 2008;**322**(5907):1516-1520. DOI: 10.1126/science.1164865

[10] Bruet BJ, Song J, Boyce MC, Ortiz C. Materials design principles of ancient fish armour. Nature Materials. 2008;**7**:748-756. DOI: 10.1038/nmat2231

[11] Jitcharoen J, Padture NP, Giannakopoulos AE, Suresh S. Hertzian-crack suppression in ceramics with elastic-modulus-graded surfaces. Journal of the American Ceramic Society. 1998;**81**(9):2301-2308. DOI: 10.1111/j.1151-2916.1998.tb02625.x

[12] Pender D, Padture N, Giannakopoulos A, Suresh S. Gradients in elastic modulus for improved contact-damage resistance. Part I: The silicon nitride–oxynitride glass system. Acta Materialia. 2001;**49**(16):3255-3262. DOI: 10.1016/S1359-6454(01)00200-2

[13] Pender D, Thompson S, Padture N, Giannakopoulos A, Suresh S. Gradients in elastic modulus for improved contact-damage resistance. Part II: The silicon nitride–silicon carbide system. Acta Materialia. 2001;**49**(16):3263-3268. DOI: 10.1016/S1359-6454(01)00201-4

[14] Giannakopoulos A. Indentation of plastically graded substrates by sharp indenters. International Journal of Solids and Structures. 2002;**39**(9):2495-2515. DOI: 10.1016/S0020-7683(02)00110-5

[15] Choi I, Dao M, Suresh S. Mechanics of indentation of plastically graded materials—I: Analysis. Journal of the Mechanics and Physics of Solids. 2008;**56**(1):157-171. DOI: 10.1016/j.jmps.2007.07.007

[16] Ruan H, Chen A, Lu J. Characterization of plastically graded nanostructured material: Part I. The theories and the inverse algorithm of nanoindentation. Mechanics of Materials. 2010;**42**(5):559-569. DOI: 10.1016/j.mechmat.2010.02.005

[17] Kot M, Rakowski W, Lackner JM, Major L. Analysis of spherical indentations of coating-substrate systems: Experiments and finite element modelling. Materials & Design. 2013;**43**:99-111. DOI: 10.1016/j.matdes.2012.06.040

[18] Choi I, Detor A, Schwaiger R, Dao M, Schuh C, Suresh S. Mechanics of indentation of plastically graded materials—II: Experiments on nanocrystalline alloys with grain size gradients. Journal of the Mechanics and Physics of Solids. 2008;**56**(1):172-183. DOI: 10.1016/j.jmps.2007.07.006

[19] Ruan H, Chen A, Chan H, Lu J. Characterization of plastically graded nanostructured material: Part II. The experimental validation in surface nanostructured material. Mechanics of Materials. 2010;**42**(7):698-708. DOI: 10.1016/j.mechmat.2010.04.007

[20] Yang DK, Cizek P, Fabijanic D, Wang JT, Hodgson P. Work hardening in ultrafine-grained titanium: Multilayering and grading. Acta Materialia. 2013;**61**(8):2840-2852. DOI: 10.1016/j.actamat.2013.01.018

[21] Lu K, Jian L. Surface nanocrystallization (SNC) of metallic materials-presentation of the concept behind a new approach. Journal of Materials Science & Technology. 1999;**15**(3):193-197

[22] Yang D, Hodgson P, Wen C. Simultaneously enhanced strength and ductility of titanium via multimodal grain structure. Scripta Materialia. 2010;**63**(9):941-944. DOI: 10.1016/j.scriptamat.2010.07.010

[23] Fang T, Li W, Tao N, Lu K. Revealing extraordinary intrinsic tensile plasticity in gradient nano-grained copper. Science. 2011;**331**(6024):1587-1590. DOI: 10.1126/science.1200177

[24] Oliver WC, Pharr GM. An improved technique for determining hardness and elastic modulus using load and displacement sensing indentation experiments. Journal of Materials Research. 1992;**7**(6):1564-1583. DOI: 10.1557/JMR.1992.1564

[25] Kot M, Rakowski W, Major L, Lackner J. Load-bearing capacity of coating–substrate systems obtained from spherical indentation tests. Materials & Design. 2013;**46**:751-757. DOI: 10.1016/j.matdes.2012.11.026

[26] Xie Z, Hoffman M, Munroe P, Bendavid A, Martin P. Deformation mechanisms of TiN multilayer coatings alternated by ductile or stiff interlayers. Acta Materialia. 2008;**56**(4):852-861. DOI: 10.1016/j.actamat.2007.10.047

[27] Wo PC, Munroe PR, Zhou Z, Li KY, Xie ZH. Effects of TiN sublayers on the response of TiSiN nanocomposite coatings to nanoidentation and scratching contacts. Materials Science and Engineering: A. 2010;**527**(16-17):4447-4457. DOI: 10.1016/j.msea.2010.03.100

[28] Zhao X, Xie Z, Munroe P. Nanoindentation of hard multilayer coatings: Finite element modelling. Materials Science and Engineering: A. 2011;**528**(3):1111-1116. DOI: 10.1016/j.msea.2010.09.073

[29] An B, Wang R, Arola D, Zhang D. The role of property gradients on the mechanical behavior of human enamel. Journal of the Mechanical Behavior of Biomedical Materials. 2012;**9**:63-72. DOI: 10.1016/j.jmbbm.2012.01.009

[30] Abdul-Baqi A, Van der Giessen E. Indentation-induced interface delamination of a strong film on a ductile substrate. Thin Solid Films. 2001;**381**(1):143-154. DOI: 10.1016/S0040-6090(00)01344-4

[31] Yang DK, Wang JT, Fabijanic D, Cizek P, Li BS, Lu JZ. Ti-based amorphous/nanocrystal composite with high ductility and strain-hardening. Materials Science and Engineering: A. 2013;**560**(10):339-342. DOI: 10.1016/j.msea.2012.09.076

[32] Green D, Tandon R, Sglavo V. Crack arrest and multiple cracking in glass through the use of designed residual stress profiles. Science. 1999;**283**(5406):1295-1297. DOI: 10.1126/science.283.5406.1295

[33] Lu K, Lu J. Nanostructured surface layer on metallic materials induced by surface mechanical attrition treatment. Materials Science and Engineering: A. 2004;**375-377**:38-45. DOI: 10.1016/j.msea.2003.10.261

[34] Lee S, Saito Y, Tsuji N, Utsunomiya H, Sakai T. Role of shear strain in ultragrain refinement by accumulative roll-bonding (ARB) process. Scripta Materialia. 2002;**46**(4):281-285. DOI: 10.1016/S1359-6462(01)01239-8